

Timo Tick

FABRICATION OF ADVANCED LTCC STRUCTURES FOR MICROWAVE DEVICES

FACULTY OF TECHNOLOGY,
DEPARTMENT OF ELECTRICAL AND INFORMATION ENGINEERING,
UNIVERSITY OF OULU;
INFOTECH OULU,
UNIVERSITY OF OULU



ACTA UNIVERSITATIS OULUENSIS
C Technica 338

TIMO TICK

**FABRICATION OF ADVANCED LTCC
STRUCTURES FOR MICROWAVE
DEVICES**

Academic dissertation to be presented with the assent of
the Faculty of Technology of the University of Oulu for
public defence in Raahensali (Auditorium L10), Linnanmaa,
on 27 November 2009, at 12 noon

OULUN YLIOPISTO, OULU 2009

Copyright © 2009
Acta Univ. Oul. C 338, 2009

Supervised by
Professor Heli Jantunen

Reviewed by
Professor Fred D. Barlow III
Professor Leszek Golonka

ISBN 978-951-42-9249-1 (Paperback)
ISBN 978-951-42-9250-7 (PDF)
<http://herkules oulu.fi/isbn9789514292507/>
ISSN 0355-3213 (Printed)
ISSN 1796-2226 (Online)
<http://herkules oulu.fi/issn03553213/>

Cover design
Raimo Ahonen

OULU UNIVERSITY PRESS
OULU 2009

Tick, Timo, Fabrication of advanced LTCC structures for microwave devices.

Faculty of Technology, Department of Electrical and Information Engineering, University of Oulu, P.O.Box 4500, FI-90014 University of Oulu, Finland; Infotech Oulu, University of Oulu, P.O.Box 4500, FI-90014 University of Oulu, Finland

Acta Univ. Oul. C 338, 2009

Oulu, Finland

Abstract

The main objective of this thesis was to research the integration of novel materials and fabrication processes into Low Temperature Co-fired Ceramic (LTCC) technology; enabling fabrication of Radio Frequency (RF) and microwave components with advanced performance. The research focuses on two specific integration cases, which divide the thesis into two sections: the integration of tunable dielectric structures and the integration of air filled waveguides.

The first section of the thesis describes the development and characterization of low sintering temperature Barium Strontium Titanate (BST) thick film paste. Sintering temperature of BST is decreased from approximately 1350 °C down to 900 °C by lithium doping and pre-reaction of the doped composition. This allows the co-sintering of the developed BST paste with commercial LTCC materials. Additionally two integration techniques to embed tunable components in an LTCC substrate using the developed BST paste are also presented and the electrical performance of the components is evaluated. The highest measured tunability value was 44% with a bias field of 5.7 V/μm. The permittivity of the films varied between 790 and 190, and the loss tangent varied between 0.004 and 0.005, all measured unbiased at 10 kHz. The developed LTCC compatible BST paste and the presented integration techniques for tunable components have not been previously published.

In the second section of the thesis, a fabrication method for the LTCC integrated air-filled rectangular waveguides with solid metallic walls is presented. The fabrication method is described in detail and implemented in a set of waveguides used for characterization. A total loss of 0.1–0.2 dB/mm was measured over a frequency band of 140–200 GHz. The electrical performance of the waveguides is evaluated and their use demonstrated in an integrated LTCC antenna operating at 160 GHz.

Keywords: embedded components, LTCC, substrate integrated waveguide, Substrate Integrated Waveguide (SIW), thick film, tunable components

Acknowledgments

First and foremost I would like to express my gratitude to my supervisor Professor Heli Jantunen for giving me the opportunity and resources to conduct this research. I also acknowledge the contribution and support of Dr. Charles Free, Dr. Tero Kangasvieri, Dr. Mikko Komulainen, Dr. Antti Uusimäki, Jyri Jäntti, Vamsi Palukuru and Jani Peräntie. Dr. Kieran Flanagan is acknowledged for revising the language of the manuscript.

I am very grateful for the staff of Microelectronics and Materials Physics laboratories for their contribution to this work and I want to thank you all for the inspiring, professional and yet fun working atmosphere.

This work was done at the Microelectronics and Materials Physics Laboratories of the University of Oulu and EMPART research group of Infotech Oulu. The work was carried out in the framework of the TAMTAM-project (2005–2008), funded by Funding Agency for Technology and Innovation (TEKES), Nokia Mobile Phones Business Group, Pulse Finland Oy, and Elektrobit Microwave Oy (2005–2006).

The work was financially supported by Tauno Tönning Foundation, Emil Aaltonen Foundation, Riitta and Jorma J. Takanen Foundation, Finnish Foundation for Technology Promotion, Infotech Graduate School, University of Oulu (2008) and Marie Curie Early Initial Training Network Fellowship of the European Community's 7th Framework Programme (PITN-GA-2008-211801-ACEOLE) (2009).

List of abbreviations and symbols

RF	Radio Frequency
LTCC	Low Temperature Co-fired Ceramic
IC	Integrated Circuit
BST	Barium Strontium Titanate
XRD	X-Ray Diffractometry
SEM	Scanning Electron Microscopy
ϵ_r	Relative permittivity
n	Tunability
T – C	Tetragonal to Cubic phase transition
T_c	Curie temperature
E	Bias field
$\tan \delta$	Loss tangent
$\tan \delta_C$	Intrinsic loss
$\tan \delta_g$	Conduction loss
PAS	Pressure Assisted Sintering
PLAS	Pressure Less Assisted Sintering
GCPW	Grounded Co-Planar Waveguide
$ S_{21} $	Transmission loss

List of original papers

This thesis is based on the following five original papers, which are cited in the text by the given roman numerals.

- I Tick T, Peräntie J, Jantunen H & Uusimäki A (2008) Screen printed low-sintering-temperature barium strontium titanate (BST) thick films. *Journal of the European ceramic society* 28: 837–842.
- II Tick T, Peräntie J, Rentsch S, Müller J, Hein M & Jantunen H (2008) Co-sintering of barium strontium titanate (BST) thick films inside a LTCC substrate with pressure-assisted sintering. *Journal of the European ceramic society* 28: 2765–2769.
- III Tick T, Palukuru V, Komulainen M, Peräntie J & Jantunen H (2008) Method for manufacturing embedded variable capacitors in low-temperature cofired ceramic substrate. *IEEE Electronics Letters* 44: 94–95.
- IV Tick T, Jäntti J, Henry M, Free C & Jantunen H (2009) LTCC integrated air-filled waveguides for G-band applications. *Microwave and optical technology letters* 51: 176–178.
- V Henry M, Osman N, Tick T & Free C (2008) Integrated Air-Filled Waveguide Antennas in LTCC for G-band operation. *Proc Asia Pacific Microwave Conference (APMC)*, Hong Kong, China.

The object of paper I was to develop barium strontium Titanate (BST) thick film paste compatible with low-sintering-temperature co-fired silver electrodes. The paper presents results of the experimental studies and characterization of the fabricated thick films. As a result, BST thick films co-fireable with silver electrodes at 900 °C were achieved.

Papers II and III both introduce a manufacturing method for the integration of the developed BST paste inside a low temperature co-fired ceramic (LTCC) substrate. The integration is achieved with pressure assisted sintering (PAS) and by using the BST paste as a via fill material. The use of both integration methods is demonstrated by an implementation of embedded variable capacitors in LTCC.

Paper IV presents a method to fabricate air-filled waveguides with solid metallic walls inside an LTCC substrate. The fabrication process is described and demonstrated. The electrical properties of the fabricated waveguides are presented.

In paper V the developed air filled waveguide fabrication methods are employed to realize antennas. LTCC integrated antennas, working at 160 GHz frequency, were fabricated and their electrical performance was measured and presented.

The author made the major contribution in developing the ideas presented in papers I–IV. Experiments and measurements were done by the author in

association with co-authors. The manuscripts for the papers I–IV, were written by the author with the kind help of the co-authors. The author’s contribution to paper V was the fabrication and structural analysis of the antennas and the associated discussion within the article.

Contents

- Abstract**
- Acknowledgments** **5**
- List of abbreviations and symbols** **7**
- List of original papers** **9**
- Contents** **11**
- 1 Introduction** **13**
 - 1.1 Functional microwave materials inside LTCC 13
 - 1.2 Substrate integrated waveguides 14
 - 1.3 Objective and outline of the thesis 16
- 2 Development of a low sintering temperature BST thick film paste** **17**
 - 2.1 BST powder preparation and characterization 17
 - 2.2 Thick film paste preparation 18
 - 2.3 Material and film structure characterization 20
 - 2.4 Electrical characterization of the BST films 21
 - 2.4.1 Temperature dependency of the relative permittivity and dielectric losses 22
 - 2.4.2 Electric field dependency of the relative permittivity and dielectric losses 24
- 3 Integration of BST thick films inside LTCC substrate** **27**
 - 3.1 Pressure assisted sintering 28
 - 3.1.1 Sample preparation 28
 - 3.1.2 Key results 29
 - 3.2 BST filled via 32
 - 3.2.1 Sample preparation 32
 - 3.2.2 Key results 33
- 4 Integration of air filled waveguides** **37**
 - 4.1 Fabrication procedure of air filled waveguides 38
 - 4.2 Fabrication of demonstrator waveguides 39
 - 4.3 Electrical performance of the demonstrator waveguides 40
 - 4.4 Application of Air filled waveguides to a substrate integrated antenna 43
- 5 Conclusions** **45**
- References** **47**
- Original papers** **51**

1 Introduction

The telecommunications industry is constantly moving towards higher frequencies and smaller product sizes, thus creating many challenges for interconnection and packaging technology. Especially the microwave and millimeter wave (mm-wave) front ends are becoming more and more complex due to the increase in devices' operational frequency and number of used frequency bands. Multilayer low-temperature co-fired ceramics (LTCC) is an established technology employed in the creation of highly integrated components and modules for microwave and mm-wave applications. It has a capability to house integrated passive circuits and 3-dimensional transmission line structures as well as to act as a reliable platform for integrated circuit (IC) assembly. In addition to its excellent integration capacity, LTCC technology offers great potential in the manufacture of multi-material modules, where materials with different electrical properties are combined within one substrate [1]. These characteristics make LTCC technology ideal for cost efficient manufacturing of future highly integrated microwave and mm-wave front end components and modules. However, there are many technical and industrial challenges still to overcome before complex LTCC modules with truly three dimensional structures and integrated functional materials can be effectively realized.

1.1 Functional microwave materials inside LTCC

Materials with high permittivity, used for capacitive components, as well as materials with magnetic permeability, used for inductive components, have been previously integrated with commercial LTCC materials [2–5]. The introduction of such materials with different electrical properties into a single package increases packaging density and devices' functionality. Today, there is increasing interests in the use of tunable dielectric materials in microwave components. Such materials, having built-in functionality, would allow the design of electrically tunable and adaptive circuits. One of the most studied and promising functional material is $\text{Ba}_x\text{Sr}_{1-x}\text{TiO}_3$ (BST), which is a ferroelectric material that is widely used as a voltage tunable dielectric in its paraelectric form.

The main challenges for the integration of a functional ceramic material in an LTCC substrate are the required low sintering temperature ($\sim 900^\circ\text{C}$) and matching the sintering shrinkage as well as the thermal expansion of the two materials. The sintering temperature of pure BST, which was chosen as the

material to be integrated, is 1350 °C and therefore the development of an LTCC compatible BST requires a drastic decrease in the sintering temperature of BST material. A lot of research has been done in order to lower the sintering temperature of BST powders below 900 °C in the past by adding various sintering aids [6–8]. Jantunen *et al.* have developed a low temperature firing BST LTCC tape and demonstrated its use with tunable microwave components [9, 10]. The co-sintering of these BST-LTCC tapes with commercial LTCC materials has also been demonstrated recently with pressure assisted sintering [11]. Besides these, no attempts to integrate tunable BST materials inside an LTCC substrate has been reported in the open literature.

When considering the manufacture of a multi material module with a BST material integrated in an LTCC, it is evident that screen printed BST thick films would allow more freedom in design compared to BST-LTCC tape layers. The functional material could be distributed freely inside the module and deposited in small areas, as opposed to having a solid layer or layers of BST covering the whole module. Besides the compatibility with LTCC materials, low sintering temperature BST thick films would offer many advantages also in hybrid microcircuit manufacturing. They would allow the use of silver as an electrode metallization instead of expensive and more resistive refractory metals. Also, lowering of the sintering temperature has been found to efficiently reduce the diffusion of barium and strontium into Al_2O_3 (alumina) and the counter-diffusion of Al-ions into BST, which can cause significant problems for electrical performance of the components [12]. Due to these reasons the development of a low sintering temperature BST thick film paste was chosen as an objective for the research into functional material integration inside LTCC in this thesis.

1.2 Substrate integrated waveguides

Nowadays, increasing numbers of applications such as collision avoidance radars [13], high-resolution radiometric imaging systems [14] and ultra-high data rate communication systems are utilizing the mm-wave frequency range above 75 GHz. Multi-chip module (MCM) technology is considered to be a solution which allows the cost efficient manufacture of such devices [15]. MCM technology allows the close integration of all the radio front end active and passive components as well as the antenna into a single module. Due to the considerable attenuation caused by the conventional planar transmission lines at such high frequencies, the substrate integrated waveguide (SIW) technology is considered

as the key building block of mm-wave MCM's [15]. SIW is an air or dielectric filled rectangular waveguide with wave propagation and isolation characteristics suitable for mm-wave operation. Structures based on SIW concepts have also been used to realize a wide range of substrate integrated waveguide components, such as filters [16–21], antennas [22, 23], phase shifters [24] and circulators [25]. The concept of SIW interconnections and components could thus be extended to form a complete low-loss transceiver module operating at high millimeter-wave frequencies.

Currently several technologies exist to realize SIW's, such as monolithic micro machining technology [26, 27], photoimageable thick film technology [16, 28] and laminated multilayer waveguide technology [29, 30]. Monolithic micro machined waveguides have a performance potential up to terahertz frequencies due to the high resolution of the photolithography fabrication process. Some of these techniques allow the integration of SIW's directly onto IC's with active circuits [27]. However, the fabrication technique, being a multi-step lithographic process, is rather expensive and also applicable only to frequencies over 300 GHz due to the restrictions imposed by the physical size of the waveguides. [15]. Dielectric filled waveguides realized with photoimageable thick film technology uses a very cost efficient and mature thick film fabrication technique suitable for mass production. The loss and dispersion properties of these waveguides have been characterized up to 200 GHz [21]. However, the increasing losses and nonlinearity of the dielectric mediums' permittivity at high GHz frequencies combined with the restrictions to the dimensions of the waveguides limit their performance and ultimately limit the frequency range in which they can be used.

Laminated waveguides, where two metallic planes are connected together by two rows of metallic posts to form a rectangular waveguide (realized with LTCC technology) offers great potential for mm-wave MCM manufacturing [29, 30]. These circuits offer high design flexibility, low cost and can be fabricated with existing mature manufacturing technology. The performance of laminated waveguides has been characterized up to 100 GHz [30]. However, similarly to the photoimageable thick film waveguides, this technology also suffers from the dimensional restrictions of the fabrication technique and also from having a dielectric filling in the waveguide. The new fabrication technology developed in this thesis will allow the integration of air-filled substrate integrated waveguides with LTCC technology [Paper IV]. The presented new technology addresses the current gap in the mm-wave spectrum, namely D, G and Y -band (110–325 GHz), where low-cost thick film and laminated waveguide techniques fail on

technological grounds and monolithic micromachining technology is too expensive.

1.3 Objective and outline of the thesis

The main objective of this thesis was to study the integration of functional materials and three dimensional fabrication processes into LTCC technology to benefit the fabrication of RF and microwave components and modules. The research focuses on two specific integration cases: integration of tunable dielectric structures and integration of air filled rectangular waveguides. The content of this thesis is summarized as follows:

In Chapter 2 the preparation of low sintering temperature BST powders and thick film pastes are presented. Thick films were printed on alumina substrates and their microstructure as well as low frequency electrical performance was then studied.

In Chapter 3 methods of integrating the prepared low sintering temperature BST thick film pastes inside an LTCC substrate are presented. Two methods have been developed to integrate BST material inside an LTCC substrate to produce voltage tunable components. Electrical properties of the components are defined up to 3 GHz.

In Chapter 4 the fabrication of air-filled rectangular waveguides with solid metallic walls inside an LTCC substrate is presented. A fabrication method for metal coating the waveguide walls is proposed and the preparation of the air-filled waveguides using existing LTCC process technology is described in detail. Electrical performance of the waveguides at 140–190 GHz was measured and the application of the waveguides in a waveguide antenna operating at 160 GHz is presented.

2 Development of a low sintering temperature BST thick film paste

An elegant method for lowering the sintering temperature of BST by pre-reaction and addition of Li_2O has been proposed by Valant *et al.* [8]. This method allows modification of the BST powders' sintering rate by varying the pre-reaction temperature. This is an important advantage, when co-sintering BST thick films inside LTCC or when sintering the films on a rigid substrate such as alumina. In the latter case the fast sintering kinetics are preferred in order to avoid diffusion between the BST and alumina and to overcome the constrictions in film shrinkage inflicted by the rigid substrate. In the former case the possibility to adjust the sintering rate allows it to be matched with that of the surrounding LTCC material. Due to these advantages the method proposed by Valant *et al.* was selected for decreasing the sintering temperature of BST powders in this work.

2.1 BST powder preparation and characterization

A commercial $0.99\text{Ba}0.55\text{Sr}0.45\text{TiO}_3 + 0.01\text{TiO}_2$ (BST) powder (Filtronic Comtek Ltd., Wolverhampton, UK) and Li_2CO_3 (Alfa Aesar GmbH & Co, Karlsruhe, Germany) as a sintering aid were used to fabricate the ceramic powders for the pastes used in these experiments. It was assumed that Li_2CO_3 decomposes to Li_2O and CO_2 during the pre-reaction. Thus, the desired doping level of Li_2O was achieved by adding the corresponding molar fraction of Li_2CO_3 . Two doping levels 0.4 wt. % and 0.8 wt. % were used. The powders were mixed in a planetary ball mill for 24 hr with ZrO_2 grinding media and acetone as a mixing vehicle. After drying, the powders were thermally treated in order to allow the reaction of Li_2O with BST. This was done at temperatures of 500 °C, 700 °C and 900 °C for 10 hours. The pre-reacted powders were then hand ground and dry-milled for 1 hr and then finally sieved. The naming convention for the powder compositions used throughout this thesis indicates the pre-reaction temperature and lithium doping. For example powder 500L04 has a pre-reaction temperature of 500 °C and a lithium (Li_2O) content of 0.4 wt. %.

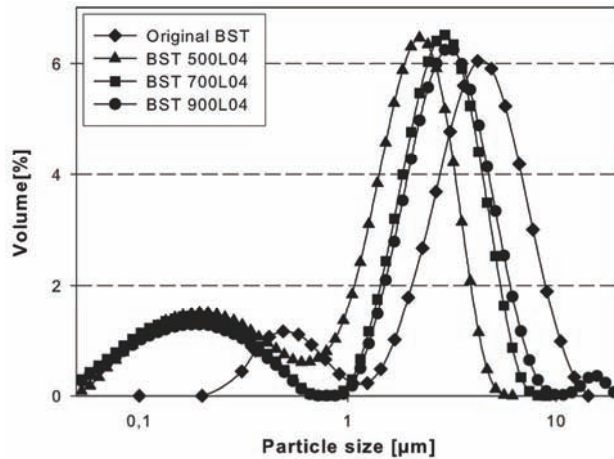


Fig. 1. Particle size distribution of three pre-reacted powders and the initial BST powder [1, published by permission of Elsevier B.V.].

The particle size distributions of the BST powders were measured with a laser diffraction particle size analyzer (LS230, Beckman Coulter Inc., California, USA). The ball milling performed before the pre-reaction reduced the average particle sizes, while the form of the particle size distribution remained relatively unchanged (Fig. 1). The increase in the pre-reaction temperature of BST with Li_2O increased the average particle size of the powders. For example the average particle size of 500L04 powder was 1.75 μm , where as the average size of 900L04 powder was 2.65 μm . [Paper I]

2.2 Thick film paste preparation

The thick film pastes used in the experiments were prepared by adding 80–83 wt. % of pre-reacted BST powders to an organic vehicle and mixing them in a triple roll mill for 30 min. In preliminary tests it was discovered that in addition to the viscosity, the solid content of the paste has a direct effect on the density of the fired film and hence will effect the relative permittivity and consequently the tunability of the films. Due to this, effort was made to maximize the solids loading in the paste without increasing the viscosity and thus compromising the printing characteristics. Two recipes R1 (83 wt. % BST powder, 17 wt. % organic medium, N485, Johnson Matthey Plc, London, UK) and R2 (80 wt. % BST powder, 16 wt. % organic medium CV-6, 4 wt. % dispersant 809, Electro science labs, Pennsylvania, USA) were used in the paste preparation. [Paper I, Paper II]

The viscosities of the pastes were measured at room temperature using a cone and plate rotation rheometer (Bohlin CS, Bohlin Reologi AB, Lund, Sweden). The BST pastes prepared with recipe R2 had a lower viscosity than the pastes prepared with recipe R1. The pastes prepared with recipe R2 were found to be easier to print and to produce better print quality in terms of surface roughness and number of pinholes. The viscosity measurements of pastes prepared with recipe R1 from 500L04, 700L04 and 900L04 powders having average particle sizes of 1.75 μm , 2.41 μm and 2.67 μm , respectively, showed that the decrease in particle size of the powders increased the viscosity of the paste. [Paper I, Paper II]

Particle size distribution of pre-reacted powders 500L04, 700L04 and 900L04 can be seen in Fig. 1. It should be noted that due to the ball milling process, the amount of very small particles ($< 0.5 \mu\text{m}$) has increased significantly. This is known to have an adverse affect on the rheological behaviour of thick film pastes. The dispersion of small particles requires an increased amount of dispersive agents and thus decreases the attainable solids loading in a paste. Additionally, very small particles are somewhat problematic during the sintering, since they tend to diffuse quickly together with bigger ones and thus leave unwanted porosity in the film. Based on this, the particle size distribution of a batch of pre-reacted powder was altered by sedimentation. The aim was to remove the smaller particles from 500L08 BST powder and thus decrease its active surface area. This was believed to allow the use of higher solids loading in the paste without increasing the viscosity of the paste and making it unprintable. Two pastes P1 and P2 were prepared from 500L08 powder and sedimented 500L08 powder, with recipe R2. The paste P1 measured viscosity of 120 Pa s, at a shear rate of 10 s^{-1} , whilst the paste P2 prepared from the sedimented powder measured a viscosity of 80 Pa s with the same shear rate. Altering the particle size (effectively the active surface area) of the powders was thus found to significantly reduce the viscosity of the paste and subsequently to allow the increase in the solids content without sacrificing the printability of the paste.

Although a comprehensive optimization of paste properties was not a part of this study, based on the performed experiments it can however be concluded that the properties of the ceramic powders and the choice of organic additives, both have great impact on the thick film paste properties. The organic additives need to be carefully chosen and matched to the properties of the used ceramic powder. The paste characteristics have a huge impact on the quality of the printed films, namely the green density and surface roughness, and consequently to the fired

density and surface roughness, thus affecting significantly the electrical characteristics of the sintered films.

2.3 Material and film structure characterization

BST films were printed directly on alumina substrates with pastes made from 500L04, 700L04 and 900L04 powders with recipe R1 and sintered at 900 °C for 2 hours. The microstructures and crystalline phases of the BST films were examined with X-ray diffractometry (XRD; Philips, Germany) and scanning electron microscopy (SEM; JSM-6400, JEOL, Tokyo, Japan). The X-ray diffraction patterns of the investigated films (Fig. 2) show that all the prepared films were clearly composed of a BST phase without detectable secondary phases. According to Valant *et al.* [8], the lithium dopant reacts with the BST forming secondary phases of Ba_2TiO_4 and Li_2TiO_3 . However, due to the low amount of lithium used in these experiments, the amount of the formed secondary phases is extremely low and consequently they were not detected in the XRD patterns. [Paper I]

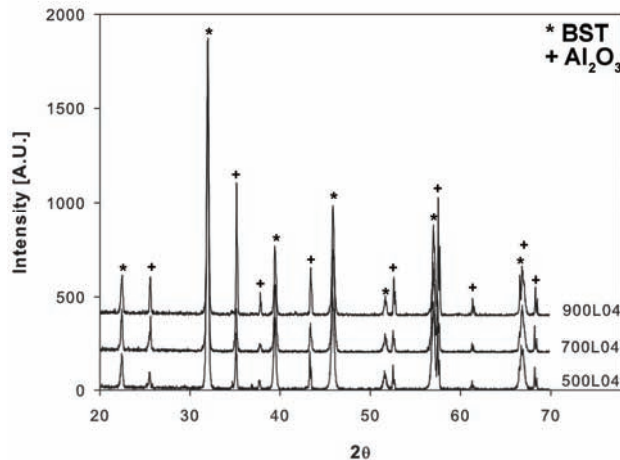


Fig. 2. X-Ray diffraction patterns of the three investigated BST films 500L04, 700L04 and 900L04. Peaks from the alumina substrate are also visible in the diffraction patterns [1, published by permission of Elsevier B.V.].

The microstructure of the printed films can be seen in SEM images (Fig. 3a–c). The density of the sintered films was estimated from the SEM images by

calculating the ratio of the BST and the void areas in the images and then transforming the area ratio to the corresponding volumetric ratio ($R_{area}^{3/2} = R_{volume}$). The area of the voids in the SEM image was differentiated from the area of the BST phase by their difference in tonal values. [Paper I]

All the fired films showed a porous microstructure. The estimated density values were 72 vol. %, 68 vol. % and 68 vol. % for the 500L04, 700L04 and 900L04 films, respectively. Although the densities evaluated from the SEM images cannot be considered as absolute values, they can be used to compare the film densities. The microstructures and the estimated density values show that, in the sintering conditions used in these experiments, the powders with the lowest pre-reaction temperature and thus the fastest sintering rate [8] yielded films with the highest density. [Paper I]

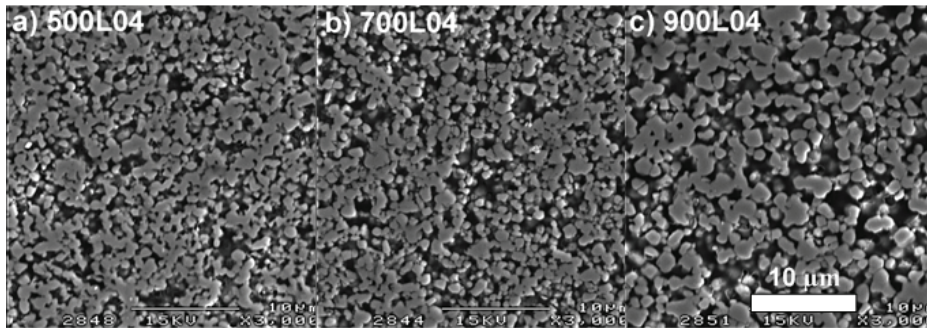


Fig. 3. SEM images of BST thick film microstructures prepared with pastes made from 500L04, 700L04 and 900L04 powders and sintered for 2h at 900 °C on an alumina substrate.

2.4 Electrical characterization of the BST films

To characterize the dielectric properties of the films, thick film parallel plate capacitors were prepared by sequentially screen printing the bottom electrode, the BST film and the 5 mm × 5 mm top electrode. A 99.6% alumina substrate was used and the films were co-sintered at 900 °C for 2 hr. Silver paste (DuPont DP6160) was used for the electrodes. The relative permittivity and loss tangent of the films as a function of bias field and temperature were measured from the parallel plate capacitor samples with a precision LCR meter (4284A, Agilent Technologies Inc., California, USA) at 10 kHz, using an external voltage source

(Agilent 6675A, Agilent Technologies Inc., California, USA) and a temperature chamber (SU-261, Espec Corp., Osaka, Japan). The thickness of the printed films was measured with a surface profiler (DekTak3ST, Veeco Instruments Inc., California, USA). Three sets of samples were manufactured using BST pastes 500L04, 700L04 and 900L04. A film thickness of 30 μm was achieved with a single print using 325 mesh screens with a 16 μm emulsion. To avoid short circuiting the pinholes in the capacitor samples, the printing was performed twice. The sintered thickness of the films in the characterization samples, varied between 56 μm and 63 μm . [Paper I]

2.4.1 Temperature dependency of the relative permittivity and dielectric losses

The relative permittivity (ϵ_r) as a function of temperature at 100 kHz was measured for all three samples. The measurements show that the ferroelectric to paraelectric (T – C) transition is very diffuse for all the samples (Fig. 4). It has been suggested that the compositional fluctuation of BST, i.e. the fluctuation of the Ba – Sr ratio in a sample, which creates phases with different Curie temperature (T_c), broadens the T – C phase transition [31]. Similar broadening of the phase transition temperature may also be due to variance in lattice distortion. According to Liou *et al.*, variation in the lattice distortion of the BST material depends on the grain size [32], and since the T_c in the BST system is proportional to the lattice constant [33], it affects the diffuseness of the T – C phase transition. As the grain size decreases, the T – C transition becomes more diffuse and both relative permittivity at T_c and tunability decreases [32]. [Paper I]

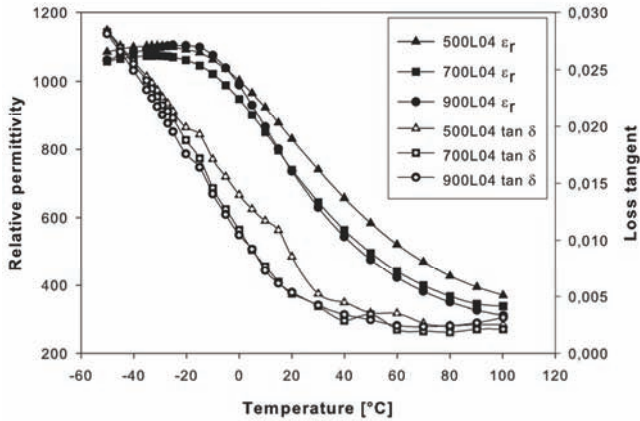


Fig. 4. Temperature dependence of permittivity and losses of the three investigated films 500L04, 700L04 and 900L04 [I, published by permission of Elsevier B.V.].

A trend of broadening of the T – C phase transition with decreasing particle size of the initial powders can be noticed in the relative permittivity measurements (Fig. 4.). The 500L04 film with the smallest initial particle size had the most diffuse T – C transition, whereas the 900L04 film with the largest initial particle size had the least diffuse transition, despite its lower density. As the density of the film decreases, the relative permittivity at T_c also decreases, and therefore the T – C phase transition of the material appears more diffuse in the relative permittivity measurements. The XRD patterns of the films did not show any signs of notable peak broadening, and thus no significant compositional fluctuation in the BST phase is expected. A possible explanation for the measured T – C transition narrowing could be grain growth during pre-reaction of the powders. Larger grain size results in a less diffuse T – C transition as stated before. The loss tangent decreases linearly with increasing temperature near the T – C transition, indicating Curie-Weiss law behaviour. The 500L04 and 700L04 films go through the T – C transition at roughly 5 °C lower in temperature than the 900L04 film. A similar decrease in the Curie temperatures with a decrease in grain size and porosity has been reported previously [34, 35]. [Paper I]

2.4.2 Electric field dependency of the relative permittivity and dielectric losses

The relative permittivities as a function of the bias field (E) are presented in Fig. 5. The relative permittivities of the 500L04, 700L04 and 900L04 films with a zero bias field were 790, 730 and 700, respectively, thus showing dependence on the density of the films. Tunability $n = (\varepsilon_r(T,0) - \varepsilon_r(T,E)) / \varepsilon_r(T,0)$ under a bias field of $3 \text{ V}/\mu\text{m}$ was 32%, 34% and 30% for the 500L04, 700L04 and 900L04 films, respectively. The tunabilities of the films were quite similar, despite the differences in the particle size of the initial powders, the film density and the permittivity at zero bias. [Paper I]

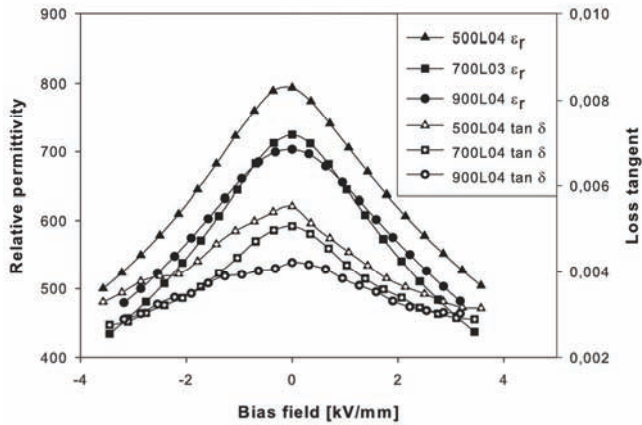


Fig. 5. Relative permittivity and loss tangent of the three investigated films 500L04, 700L04 and 900L04 as a function of bias field, measured at 10 kHz [1, published by permission of Elsevier B.V.].

Measurement of loss tangent ($\tan \delta$) as a function of the bias field showed behaviour similar to that of the relative permittivity (Fig. 5). The losses were also found to be in a good agreement with the density of the films: the more porous the films, the lower the dielectric losses. The loss tangents of the films with a zero bias field were measured to be 0.0042, 0.0051 and 0.0055 for the 500L04, 700L04 and 900L04 films, respectively. [Paper I]

It is assumed that the dielectric losses of the BST films in the paraelectric state can be solely attributed to intrinsic ($\tan \delta_C$) and conduction ($\tan \delta_R$) loss mechanisms. The total dielectric loss of a material is the sum of these two previous mechanisms, which have opposing behaviours as a function of the DC

field; with an increasing electric field the intrinsic loss decreases while the conduction loss increases. Both loss mechanisms are also temperature dependent through the variation of permittivity against temperature. When the temperature rises just above the Curie point, the permittivity is high and the intrinsic loss dominates over the negligible conduction loss component. Hence, the total loss decreases with an increasing bias field. At higher temperatures, the intrinsic loss decreases rapidly and the effect of the DC field on the intrinsic losses is suppressed. This leads to an increase in the effect of the conduction loss on the total loss and hence the total loss begins to increase with an increasing bias field. [36][Paper I]

The developed low sintering temperature BST thick films have been applied in the manufacture of numerous different tunable RF and microwave components [37–39]. As a part of these experiments the high frequency electrical properties of the films have been characterized with a method described here [40]. The permittivity of a film printed with a paste made from powder 500L04 with recipe R1 at a frequency range of 1–6 GHz was approximately 400 with slight decrease as a function of frequency. The loss tangent of the same film was between 0.02 and 0.05, which increased as a function of frequency. A significant decrease in the relative permittivity and an increase in the loss tangent was observed when compared to the results measured at 10 kHz. The tunability, however, remained fairly constant at 25% and was measured with 2.5 V/ μm bias field over the whole frequency range of 1–6 GHz. [37]

3 Integration of BST thick films inside LTCC substrate

The main challenges in the integration of functional ceramic materials inside an LTCC substrate are the requirements of matching sintering temperature and sintering shrinkage. Additionally, the differences in coefficient of temperature expansion or diffusion between the materials can cause problems for the integration. The preliminary experiments that were done to co-sinter BST thick films with LTCC tapes resulted in heavily deformed samples. The films printed on a stack of LTCC tapes bent the whole structure, whereas the films placed in the middle of the LTCC tape stack in a symmetrical manner to avoid the deformation partially dissolved into the glass matrix of the LTCC tape. It was clear that very fast sintering kinetics were required from the BST material to overcome these problems.

The bulk of the commercial LTCC tape systems are glass ceramic composites. In such systems the low sintering temperature is achieved by the presence of a liquid phase during the sintering process. These materials contain a significant amount of low melting point glass, which after it has been melted, allows the ceramic particles to move easily and to form a dense microstructure. The liquid phase present during sintering allows the use of very short sintering times. When developing a low sintering temperature tunable BST material the use of a continuous glass phase to enhance densification at low temperatures is however restricted. The presence of a continuous glass phase would result in the concentration of the biasing electric field in the lower permittivity glass instead of the higher permittivity BST and therefore impair the tunability of the material. Additionally it would be very challenging to find a glass material that would not react with the BST at sintering temperatures while still having a suitable melting point and wetting characteristics. Due to these restrictions, the addition of glass into the BST paste to allow liquid phase sintering was rejected, and consequently the sintering rate of the BST material could not be matched to that of the LTCC system. The challenges inflicted by the inherently different sintering shrinkage properties of the BST and commercial glass-ceramic composite LTCC materials are thus tackled differently with two methods: with the use of pressure assisted sintering [Paper II] and with very localized BST coverage as a form of a via filled with BST paste [Paper III].

3.1 Pressure assisted sintering

Screen printed thick films have large dimensions (mm) in the x and y directions and small dimensions in z-direction (μm). When printing films that shrink during sintering on a non-rigid platform that also shrinks, even the slightest mismatch in sintering shrinkage of those two materials can result in a significant difference of the dimensions over large areas and therefore deform the structure. In the case of integrating BST thick films sintered inside LTCC, if the sintering shrinkage could be allowed only to happen in the z direction, where the dimensions of the film are very small (order of tens of μm), the deformation caused by the mismatch in sintering shrinkages could largely be avoided.

A pressure-assisted sintering (PAS) technique, where constraining layers of Al_2O_3 green tapes are laminated on both sides of an LTCC laminate and uniaxial pressure is continuously applied during co-firing to restrict shrinkage in the x and y directions, has been used to achieve zero-shrinkage sintering [41]. This way the shrinkage of materials is forced in the z-direction and zero x and y directional shrinkage is achieved. Additionally, the x and y dimensional shrinkage tolerances are also significantly reduced compared with those of the free sintering process. Similar pressure-assisted sintering (hot pressing) has also been used to co-sinter mixed-material ceramic-ceramic structural composites where the materials have mismatching sintering behaviours [42]. In this work the pressure assisted sintering is applied to overcome the mismatch of sintering shrinkage between BST and commercial LTCC tape and thus allow the integration of screen printed BST films inside LTCC substrate.

3.1.1 Sample preparation

Thick film parallel plate capacitors were prepared inside an LTCC substrate. The sample structure is presented in Fig. 6. The effective electrode area of the capacitor structure was $2.5 \text{ mm} \times 2 \text{ mm}$ (5 mm^2). A DuPont 951 LTCC tape system ($\epsilon_r = 7.8$, $\tan \delta = 0.0015$ at 10 MHz) was used with DuPont 6142D silver pastes. BST paste was prepared from 500L08 powder with recipe R2. A powder with a low pre-reaction temperature and high lithium content was selected so that the sintering rate of the BST film would be as fast as possible. [Paper II]

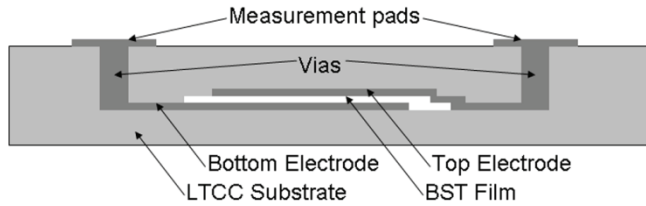


Fig. 6. Structure of the LTCC integrated BST varactor used in the measurements [II, published by permission of Elsevier B.V.]

The LTCC tapes were cut into 88 mm × 88 mm sheets and 200 μm via holes were drilled with a laser (Siemens Microbeam 3200, Siemens, Germany). The vias were filled with DuPont 6141 silver via fill paste. The electrodes and the BST films as well as probe contacts on the top layer were sequentially printed on the LTCC tapes. The printing of BST paste was performed twice to avoid pinholes. The printed LTCC tapes (DuPont 951PX) were aligned and stacked and finally laminated together with restrictive alumina tapes (DuPont 951RT). The laminated panel consisted of five 256 μm thick layers. Sintering times of 30 min and 60 min were used with pressures of 0.5 MPa, 1 MPa and 2MPa (PEO 603, ATV Technologies). [Paper II]

The microstructure of the films was examined with scanning electron microscopy. The density of the sintered films was estimated from the SEM images as described in chapter 2.3. The thicknesses of the sintered films were measured from cross-sections with an optical microscope measurement system (BX51, Olympus, Tokyo, Japan). Electronic properties of the films were measured as described in 2.4.

3.1.2 Key results

Visual inspection revealed that the samples sintered under a pressure of 0.5 MPa had severe cracks, whereas the samples sintered under pressures of 1 MPa or 2 MPa were found to be undamaged. LTCC samples of the same thickness with restrictive alumina tapes have been successfully sintered without applied pressure to achieve zero shrinkage sintering (Pressure less assisted sintering, PLAS). Thus it is evident that the introduction of a material with unmatched sintering shrinkage and sintering rate restricted the sintering conditions instead of the introduction of restrictive alumina tapes. Sufficient pressure is therefore needed during sintering to overcome the stresses inflicted on the LTCC substrate by the different shrinkage behaviour of the BST film. [Paper II]

The estimated density values of the integrated films are presented in Table 1. These results show that the films sintered for 60 min had approximately 5 vol. % higher density than the films sintered for 30 min. The influence of the applied pressure on the density during sintering could not be detected. The thickness of all the films, measured from the microscopic images, was approximately 35 μm . However, the accuracy of the measurement method did not allow the film thickness to be defined with enough precision to find a correlation between the sintering conditions and the film thickness. [Paper II]

Table 1. Densities of the integrated films analyzed from SEM images.

Density [vol. %]	Sintering time	
	30 min	60 min
Sintering pressure		
0.5 Mpa	(S305) 58%	(S605) 62%
1 Mpa	(S301) 57%	(S601) 60%
2 Mpa	(S302) 55%	(S602) 60%

The dielectric properties of the sintered films were measured from the parallel plate capacitor samples. As mentioned above, the samples sintered using 0.5 MPa pressure had visible cracks. Due to this, proper electrical contact with the electrodes was not established and measurement of the samples was impossible. In addition, it was found that the samples sintered under a pressure of 2 MPa were all short-circuited. The high sintering pressure overloaded the samples, which forced the silver electrodes to penetrate the BST film, resulting in defects and short circuits. The sintering pressure of 1 MPa produced structurally and electronically functional samples. [Paper II]

Possible reasons for the film defects under high and low sintering pressures might be the unequal sintering pressure due to the unevenness of the laminated LTCC panel surface. The fabricated parallel plate capacitors were composed of two $\sim 10 \mu\text{m}$ thick electrodes and a $\sim 35 \mu\text{m}$ thick BST film, thus having a total thickness of $\sim 55 \mu\text{m}$. After lamination the buried capacitors were clearly visible as bumps on the LTCC panel surface. Therefore, it can be assumed that the actual pressure formed at the bump locations, when the LTCC panel is pressed between the flat sintering plates, is significantly higher than in the bump surroundings. The pressure used during sintering of a multi-material LTCC module should thus be carefully adjusted and further research is needed to define the optimal sintering conditions. [Paper II]

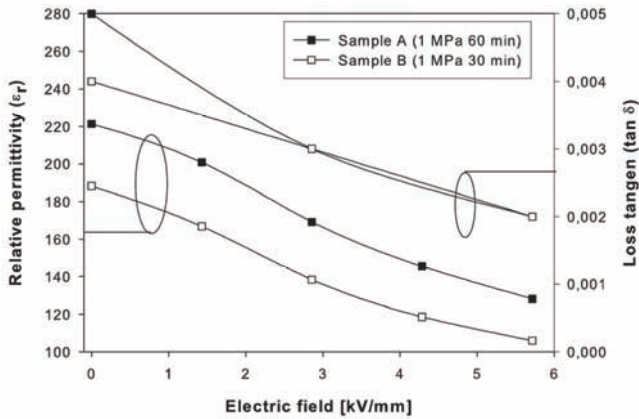


Fig. 7. Dielectric properties of the LTCC integrated BST film samples S301 and S601 measured at 10 kHz [11, published by permission of Elsevier B.V.].

The measured dielectric data of the LTCC-embedded BST films is presented in Fig. 7. The unbiased relative permittivity of the samples sintered under a pressure of 1 MPa for 60 min (sample S601) and 30 min (sample S301) was 220 and 188, respectively at 10 kHz. This agrees well with the presented porosity estimations of the films and indicates that sintering time has a significant effect on sintered density and furthermore on relative permittivity. The ϵ_r of samples S601 and S301 decreased to 128 and 105 at 10 kHz when the biasing field was increased from 0 to 5.7 V/ μm . Thus, the tunability n of samples S601 and S301 was 42% and 44%. The loss tangent of the films S601 and S301 at zero bias field was 0.005 and 0.004, respectively at 10 kHz. The loss tangent ($\tan \delta$) of a thick film BST capacitor decreased as the DC bias field increased, as illustrated in Fig. 7. Loss levels are similar to the levels of the unburied films presented earlier, in spite of the higher lithium content and the use of pressure-assisted sintering. The relative permittivity of the buried films is significantly lower than in the unburied films. This is most likely due to the higher lithium content in the BST powder. It has been shown that the increase in the lithium doping in the pre-reacted BST powder effectively decreases the relative permittivity [8]. Also the measured porosities of the buried films were higher than the ones in the unburied films, which would adversely affect the relative permittivity. However, it has to be remembered that due to the characteristics of the measurement system, the porosity results between these two sets of samples might not be fully comparable. Tunabilities of both the buried and unburied films with 3 V/ μm bias field were $\sim 25\%$ and 30–34%,

respectively. Thus, it can be said that the observed large decrease in relative permittivity had only a marginal effect on the tunability of the films. [Paper II]

3.2 BST filled via

In the previous chapter the problem of mismatching sintering shrinkages of BST thick films and LTCC materials was solved by forcing the sintering shrinkage in z-direction where the film has small dimensions. Due to the restrictions of screen printing technology it is difficult to achieve such small (tens of micrometers) magnitude repeatably in the x and y dimensions. These dimensional restrictions also result in production difficulties of parallel plate or interdigital varactors with a small capacitance. The high relative permittivity of the BST material would require the use of electrodes with dimensions below the capabilities of the standard screen printing process. The vias connecting the conductive patterns on different layers in multilayer ceramic circuits typically have dimensions that meet the criteria described above. Conductive vias of a size in the order of a few tens of micrometers are being produced consistently [43, 44] and the techniques used to fabricate conductive vias can be readily be employed to nonconductive materials. This has been previously presented in the fabrication of resistors, capacitors and ferromagnetic elements [45–47]. In this section a fabrication method of LTCC integrated BST varactors, that is based on vias filled with BST material is presented.

3.2.1 Sample preparation

Fig. 8 shows a cross-section of the designed varactor component. A BST-filled via is placed between the signal line and the bottom ground plane of a 50 Ω grounded coplanar waveguide (GCPW) transmission line. In the designed structure the via diameter (d) is 200 μm and the height (h) is 50 μm . The unbiased capacitance of the varactor can be varied by changing the diameter of the BST-filled via. To ensure proper grounding, the ground traces on the substrate are connected to the bottom ground plane with multiple conducting vias. The top side grounding is opened around the top electrode of the BST-filled via to decrease unwanted parallel signal-to-ground capacitances, which would impair the tunability of the varactor. [Paper III]

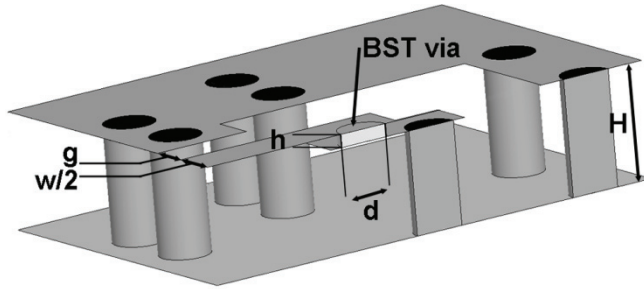


Fig. 8. Designed structure and dimensions of the BST varactor via: $g = 200 \mu\text{m}$, $w/2 = 100 \mu\text{m}$, $d = 200 \mu\text{m}$, $h = 50 \mu\text{m}$ and $H = 500 \mu\text{m}$ [III, published by permission of IEEE/ET].

The varactor was fabricated by injecting BST paste into laser-drilled via holes of LTCC green tapes in a similar manner as the conductive pastes are used for via filling in the standard process. Silver electrodes were then printed on the top and bottom sides of the BST-filled vias. The paste used in via filling was prepared from powder 500L04 with recipe R1, except that the viscosity of the paste was adjusted to match the requirements of via filling, by increasing the ceramic content. DuPont 951 LTCC dielectric tape ($\epsilon_r = 7.8$, $\tan \delta = 0.0015$ at 10 MHz) and compatible silver thick film and via pastes were used in the experiments. [Paper III]

3.2.2 Key results

A cross section of the fabricated varactor component with a BST-filled via is shown in Fig. 9. Some swelling of the via can be detected, which is caused by overfilling of the via with the BST paste. It is difficult to avoid overfilling when fabricating vias with a high aspect ratio (d/h). The fabricated via shown in Fig. 9 has an aspect ratio of 4, which is at the upper limit of the fabrication technique. This limits the use of the fabrication method to only small capacitances. [Paper III]

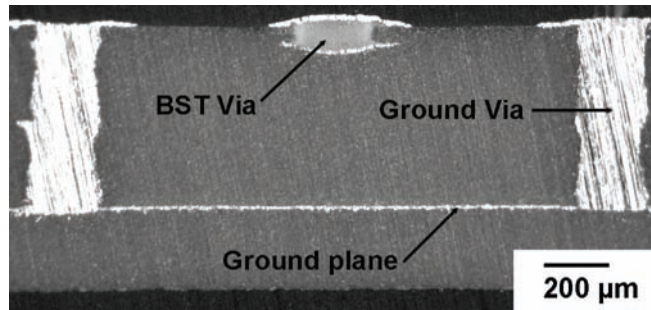


Fig. 9. A cross section of the fabricated LTCC embedded BST varactor via [III, published by permission of IEEE/ET].

The S-parameters of the tunable capacitors were measured with an (HP 8719C, Agilent Technologies Inc., California, USA) network analyzer using a probe station with 450 mm pitch probes. An external bias-T component and voltage source (Agilent 6675A, Agilent Technologies Inc., California, USA) were used to apply a bias field over the ferroelectric via.

Fig. 10 shows the measured capacitances and Q factors of the fabricated varactor component with bias voltages applied in 50 V increments from 0 V to 200 V (bias field $E \sim 0 \text{ V}/\mu\text{m}$ to $4 \text{ V}/\mu\text{m}$). As a result of the increase in bias voltage the capacitance of the varactor, measured at 1 GHz, changed from 1.47 pF to 0.97 pF and the calculated maximum tunability n was thus 34%. The Q factor at 1 GHz and the self-resonant frequency of the varactor increased from 18 to 32 and 6.3 GHz to 7.7 GHz, respectively, as the bias voltage was increased from 0 to 200 V. [Paper III]

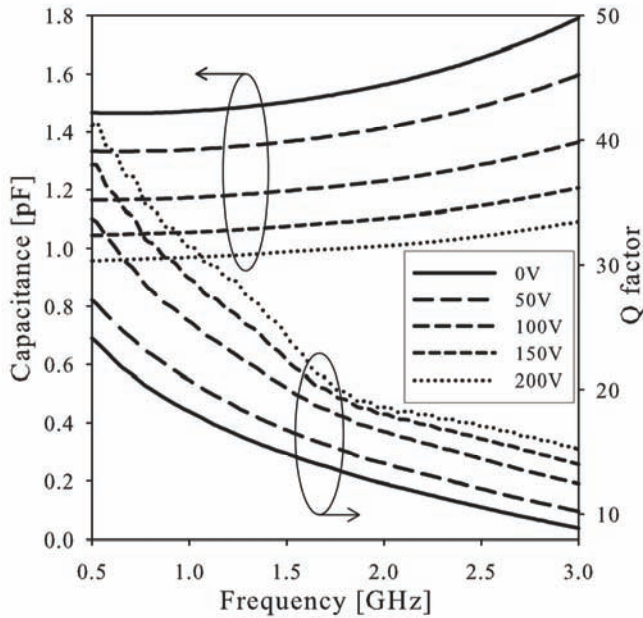


Fig. 10. Measured capacitance and Q-factor of the LTCC embedded BST varactor [III, published by permission of IEEE/IEE].

The unbiased capacitance of the varactor can be easily changed by choosing different via sizes. With the currently used BST paste ($\epsilon_r \sim 260$ @ 1 GHz) and tape thickness of 50 μm , capacitances ranging from approximately 0.1 pF to 1.5 pF can be produced by adjusting the BST via diameter from 50 μm to 200 μm . The tunability of the varactor can be further enhanced by increasing the biasing field in the BST material. This increase can be realized either by increasing the bias voltage or by decreasing the height of the BST via by using thinner LTCC tape. However, the electric field dependence of the BST material is not linear, and the effect of the increase in the bias field on the relative permittivity will eventually saturate. [Paper III]

The Q factor of the varactor presented in Fig. 10 reflects the electrical properties of the BST material. The Q factor decreases as the frequency increases or the bias voltage decreases. These changes are due to the decrease in the dielectric losses of the BST material under an increase in the biasing field or a decrease in frequency, and they are inherent properties of the material. [Paper III]

4 Integration of air filled waveguides

Previously substrate integrated waveguides have been fabricated inside an LTCC by using via fences as waveguide walls [30]. These laminated waveguides have the inherent drawback of non-continuous waveguide side walls that allow the leakage of the microwave power from the periodic gaps in the via fence. The key attributes that define the leakage characteristics of a laminated waveguide for a given frequency are: via size, via spacing and waveguide width to height ratio [48]. The vias should be placed as closely together as possible and also the via diameter to waveguide width relation should be minimized to avoid the dispersion of the propagating wave in the waveguide [48]. These restrictions in electrical design combined with the dimensional limitations inflicted by the LTCC fabrication process, set the upper limit for the frequency where laminated waveguides can be used.

A ‘rule of thumb’ has been established that the via spacing of a laminated waveguide should be less than a quarter wavelength, to eliminate the effect of radiation leakage on the attenuation of a signal [30, 49]. For a waveguide, working for example at a frequency of 200 GHz, that would mean roughly a 370 μm via pitch, which is within the current LTCC manufacturing standards. However, the relatively high ϵ_r of the LTCC dielectric, for example of Du Pont 951 whose ϵ_r is 7.8, would result in a WR5 (width 1.30 mm, height 0.65 mm) waveguide with a width of 167 μm and a via diameter to waveguide width relation of almost one, which are both unacceptably small. The concept of an LTCC integrated air filled waveguide with solid metallic walls largely eliminates the problems and limitations associated with the laminated waveguides described above. Air filled channels and cavities inside LTCC have been previously applied for example in micro fluidic systems and various cavity fabrication methods are thus well known [50–53]. Air as a medium inside the waveguide, in which the electromagnetic wave propagates, has significantly lower dielectric loss than any ceramic material, which reduces the attenuation of the waveguide. Additionally, the low permittivity of air allows the physical size of the waveguides, operating in high mm-wave spectrum (D, G and Y band, 110–325 GHz), to remain in the range where they can be repeatably fabricated with the LTCC process.

4.1 Fabrication procedure of air filled waveguides

The fabrication of integrated air-filled waveguides begins with the preparation of three elements: top, middle and bottom, shown in Fig. 11. The LTCC green tapes for the elements are cut and the required conductor patterns and vias are produced for the secondary circuits. The waveguide shape is cut in the tapes forming the middle element. The green tapes for each element are then aligned and stacked. The three elemental sections are laminated individually keeping the lamination conditions identical to ensure matching sintering shrinkage of the elements after the final lamination. [Paper IV]

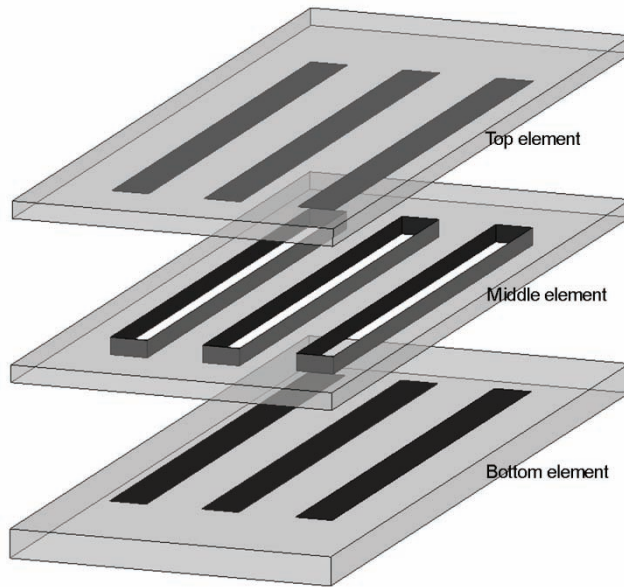


Fig. 11. Schematic of the elements constituting an LTCC integrated air-filled waveguide [IV, published by permission of John Wiley & Sons, Inc.].

After lamination, the metallizations to the top and bottom elements of the waveguide, hereafter referred to as planar metallizations, are done by screen printing. The metallizations are printed on the top of the bottom element and on the bottom of the top element. The procedure to apply metallization to the waveguide walls, hereafter referred to as vertical metallization, (i.e. pull through printing) is shown schematically in Fig. 12. The waveguide opening in the middle element is first filled with a conductive paste through a stencil. Then the excess conductive paste is removed by peeling off the base foil underneath the middle

element. A thin coating of conductive paste thus remains on the waveguide walls. Alternatively, the vertical metallizations can be applied to individual LTCC tapes, before aligning and stacking the middle element. When operating in such a way, it is recommended that the stencil used for filling the waveguide opening should be slightly larger than the opening itself. This way a narrow band of conductor paste is also deposited on the top surface of each individual LTCC tapes, which ensures proper electrical contact between sheets after stacking. The electrical conductivity of the waveguide walls in the vertical direction is critical for the effective functioning of the waveguide, since large currents propagate in the waveguide in this direction. [Paper IV]

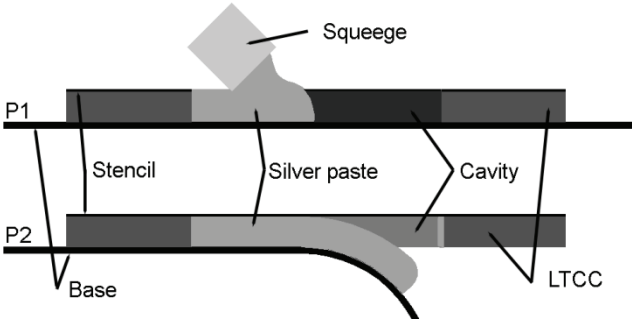


Fig. 12. Vertical metallization procedure of the waveguide walls: P1: Filling of the waveguide with metallic paste, P2: Peeling off the base foil [IV, published by permission of John Wiley & Sons, Inc.].

After the planar and vertical metallizations have been applied, the three elemental sections are aligned and stacked. It was found that this was best done before the conductive paste on the elements was dried. In this way the metallizations on each element adhere to each other and a uniform electrical conductivity around the waveguide is achieved. The three stacked element sections are then laminated to form a single LTCC panel and finally fired. [Paper IV]

4.2 Fabrication of demonstrator waveguides

The demonstrator waveguides were fabricated by using the DuPont 951 LTCC tape system. The tapes were cut to 88 mm x 88 mm sheets and the via holes for alignment, as well as the cavity for the waveguide section were laser cut. The designed dimensions of the cavity are presented in Fig. 13. [Paper IV]

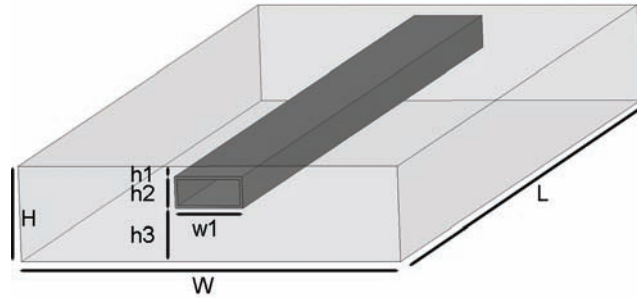


Fig. 13. Structure and dimensions of the demonstrator waveguide. $H = 1.815$ mm, $W = 7$ mm, $L = 10$ mm, 20 mm and 30 mm, $h1 = 0.2$ mm, $h2 = 0.615$ mm, $h3 = 1$ mm and $w1 = 1.3$ mm [IV, published by permission of John Wiley & Sons, Inc.].

A mould of identical size as the waveguide cavity was made and a silicone insert was cast for the lamination of the cavity part. The top, bottom and cavity parts were then laminated at 20.7 MPa and 70 °C for 10 minutes. Silver thick film paste (DP6142D, DuPont) was used for the planar and vertical metallizations. For the vertical metallization the paste was thinned by adding α -terpineol. The viscosity of the thinned paste was measured to be 40 Pa·s at the shear rate of 10 1/s. The metallized parts were then aligned and stacked. The final lamination of the three parts was done with uniaxial lamination at 10 MPa and 70 °C for 20 minutes. The laminated panels were then sintered at 875 °C for 20 minutes bottom side up, to avoid the collapse of the thin top part. An extremely slow heating profile, with a long burnout time was used to allow the combustion gasses to exit the cavity without causing deformation. Finally, waveguides of three different lengths, 10 mm, 20 mm and 30 mm, were cut out of the sintered panels for electrical measurement. [Paper IV]

4.3 Electrical performance of the demonstrator waveguides

Diagonal and perpendicular cross sections of the fabricated waveguides are presented in Fig. 14 and Fig. 15. The width and height of the waveguides after sintering were 1.2 mm and 0.56 mm. The final dimensions were smaller than the designed width 1.30 mm and height 0.65 mm (WR5). The thickness of the metallizations was not taken into account when cutting the waveguide slots on the tapes, which was the main cause for the difference in designed and realized dimensions. Using pull through printing it is very difficult to exactly control the thickness of vertical metallization. The surface roughness of the planar

metallizations was measured to be $0.6\ \mu\text{m}$. The surface roughness of the vertical metallizations could not be measured. [Paper IV]

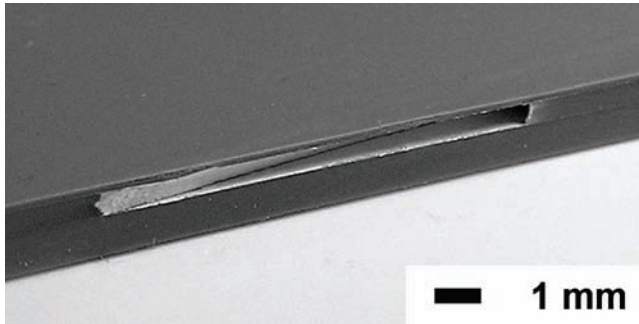


Fig. 14. Diagonal cross-section of the fabricated waveguide [IV, published by permission of John Wiley & Sons, Inc.].

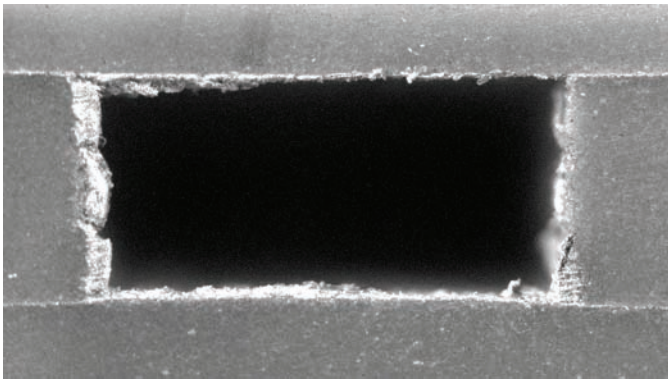


Fig. 15. Orthogonal cross-section of the fabricated waveguide [IV, published by permission of John Wiley & Sons, Inc.].

The S-parameters of each of the fabricated sections were measured using a vector network analyzer covering the frequency range 140–200 GHz. The LTCC air-filled waveguide sections were fitted with flanges that were aligned with the WR5 waveguide outputs. As previously mentioned, three waveguide sections of different lengths (10 mm, 20 mm and 30 mm) were fabricated, and the transmission loss ($|S_{21}|$) through each section were measured. By computing the differences in loss through the three sections, the loss permit length (dB/mm) was

obtained. This difference technique was used to overcome problems associated with loss in the measurement system. [Paper IV]

The measured attenuation in the fabricated waveguides is shown in Fig 16. At 150 GHz, a total loss of 0.13 dB/mm was measured. Using standard theory for rectangular metallic waveguides, a much lower loss/mm is obtained. But this is not a very meaningful comparison, because the standard theory ignores skin effects and more importantly the surface roughness. It is the losses due to surface roughness that will dominate the attenuation performance in waveguides at millimeter-wave frequencies. [Paper IV]

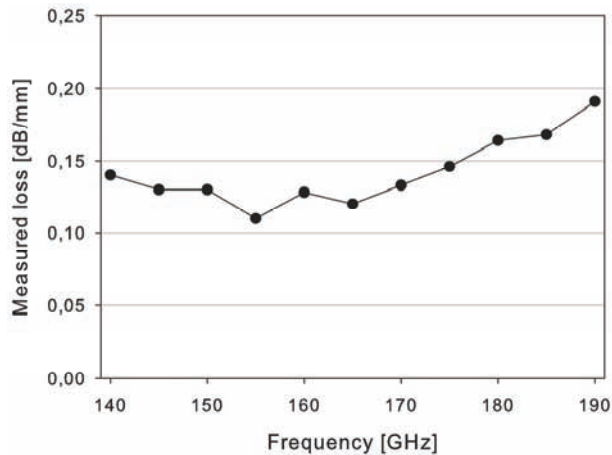


Fig. 16. Measured transmission loss permit length of the fabricated demonstrator waveguides [IV, published by permission of John Wiley & Sons, Inc.].

The direct performance comparison between the air-filled laminated waveguides presented here and the laminated waveguides presented in the literature is impossible, since no measurement data of the laminated waveguides at 140–190 GHz frequency exists. If the measured total loss of 0.13 dB/mm of the air-filled waveguides is viewed against the total loss of 0.07 dB/mm measured from the laminated waveguide at 75–90 GHz [30], the benefits of this inherently more complex fabrication technique may not be so obvious. However, it has to be remembered that the air-filled waveguides presented and measured here operate at frequencies two times higher and that the realization of laminated waveguides for these frequencies with LTCC technique is simply impossible due to their physical size. Furthermore, since the experiments made here were the first of their kind, it

can be expected that the performance of the waveguides can still be improved by further improving the manufacturing process to produce air filled waveguides with tighter dimensional tolerances and vertical metallization with lower surface roughness and better thickness control. [Paper IV]

4.4 Application of Air filled waveguides to a substrate integrated antenna

To demonstrate the potential of the technology, a substrate integrated 160 GHz waveguide antenna was fabricated and measured. The air-filled waveguide antenna consisted of a short circuit terminated waveguide, with an array of slots in the broad wall of the waveguide to give in-phase radiation. The waveguide antenna was fabricated using the techniques and dimensions presented in the previous chapter. The radiating slots were laser drilled after sintering the waveguide. A picture of an LTCC integrated antenna is presented in Fig. 17. [Paper V]

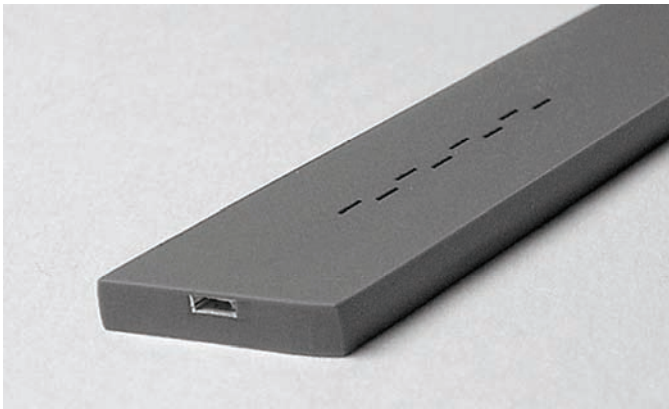


Fig. 17. Fabricated LTCC integrated 160 GHz waveguide antenna.

The fabricated waveguide antenna was connected to the measurement system as previously done in the waveguide attenuation measurements. The measured return loss of the antenna is plotted in Fig. 18, and it shows a good match, very close to the design frequency of 160 GHz. [Paper V]

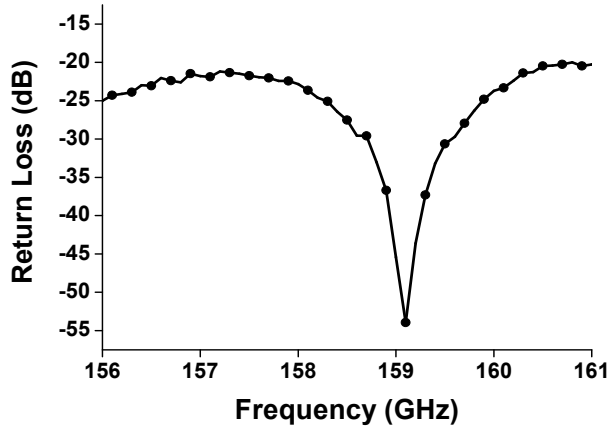


Fig. 18. Measured return loss of the LTCC integrated waveguide antenna [V, published by permission of APMC].

The slight shift in the operation frequency (0.6%) can be attributed to imperfectly realized antenna dimensions. Sintering shrinkage of the LTCC tapes and the metal coating thickness in the waveguide walls are difficult to predict precisely. These variations may have affected the operating frequency of the antenna. In addition, the tolerances in the alignment of the radiating slots relative to the waveguide may have shifted the operating frequency. To ensure the proper functioning of the antenna the radiation patterns were also measured. The measured beam width and gain values agreed well with the theoretical predictions. As expected the gain was slightly less than that from an 8-slot in a pure metallic waveguide. This will be mainly due to the losses in the conductor walls. The gain could be improved by decreasing the surface roughness of the waveguide walls. The results of the antenna measurements are covered in more detail in [Paper V].

5 Conclusions

The main target of this thesis has been to study the integration of new materials and fabrication processes into LTCC technology to benefit the fabrication of advanced performance RF and microwave components. The study focuses on two specific integration cases, which divide the thesis into two sections: integration of tunable dielectric structures and integration of air filled waveguides.

The first section of the thesis describes the development and characterization of a low temperature firing BST thick film paste. The sintering temperature of the BST powder was lowered to 900 °C with lithium doping and pre-reaction at temperatures between 500 °C and 900 °C. This enabled the co-sintering of the developed BST with a commercial LTCC material. Thick film pastes were produced and characterized from the low sintering temperature powders.

The microstructure and electrical performance of the sintered BST thick films were characterized for films printed on an alumina substrate. All the prepared films were clearly composed of a BST phase without detectable secondary phases. Porosity of the films was estimated to be between 68% and 72% and inversely related to pre-reaction temperature. The powders with lowest pre-reaction temperature produced the films with highest density. The relative permittivity of the films printed on an alumina substrate varied between 790 and 700 at 10 kHz, depending on the pre-reaction temperature. Total loss of the films was between 0.004–0.005 at 10 kHz. The films exhibited tunability of 30–34% with an applied bias field of 3 V/μm. Based on these results it can be concluded that lithium doping of BST with pre-reaction at elevated temperatures is an effective method to decrease the sintering temperature of BST powders for LTCC compatible screen printed thick film pastes.

Integration of the BST thick films inside an LTCC substrate was achieved with pressure assisted sintering. The electrical properties of the embedded films were characterized from varactors fabricated inside an LTCC substrate. The films had a relative permittivity of 188–220 depending on the sintering time. The loss tangents of the films varied between 0.004 and 0.005. The films exhibited a tunability of 42–44%, under a bias field of 5.7 V/μm. Sintering conditions were optimized by varying the sintering time and applied pressure. Based on these experiments, it can be concluded that pressure-assisted sintering enables co-firing of BST thick films with LTCC materials. By choosing the correct sintering conditions (time, temperature and pressure) mechanically and electronically functional components were produced. Pressure assisted sintering was found to be

a useful method to integrate thick films with mismatching sintering-shrinkage properties inside an LTCC substrate.

A method for manufacturing small sized variable capacitors inside an LTCC substrate was presented and validated through a practical implementation and measurements. The capacitance and Q factor of the fabricated varactor component changed from 1.47 pF to 0.97 pF and 18 to 32, respectively, at 1 GHz, with 200 V bias voltage. (4 V/ μm bias field) The calculated maximum tunability was 34%. The presented method allows the fabrication of integrated, small-sized, small capacitance varactors inside an LTCC substrate in large quantities with the existing standard LTCC fabrication process.

In the second section of this thesis a fabrication method of LTCC integrated air filled rectangular waveguides with solid metallic walls, applicable for D, G and Y band (110–325 GHz) applications was presented. The fabrication method was described and a set of waveguides was prepared for electrical characterization. The electrical performance of the waveguides was evaluated at 140–190 GHz frequency. The measured total loss of the waveguides was 0.13 dB/mm at 150 GHz.

The use of the waveguides was demonstrated in a 160 GHz LTCC integrated antenna. The air-filled waveguide antenna consisted of a short circuit terminated waveguide having an array of slots in the broad wall of the waveguide. The successful integration of the antenna structure demonstrated the feasibility of the fabrication process. Overall, the results have established the concept of the integrated air filled waveguide antenna with solid metallic walls. The presented concept allows the manufacturing of substrate integrated waveguides for higher frequencies than with the existing techniques.

The results and techniques reported in this thesis, have demonstrated the potential advantages of materials integration and three dimensional processes in the manufacturing of microwave LTCC components. Both sections of the thesis present results from the very first attempts to realize these novel techniques. Therefore significant improvements in the measured performances of components made with these techniques are expected with further optimization of the manufacturing process. The electrical characterization of BST films at high GHz frequencies would enable its use in combination with air-filled waveguides to form integrated and tunable mm-wave circuits. Thus, in the future, the concept of air-filled interconnections could be extended for example to form a complete low-loss transceiver, with an integrated phased array antenna operating at high millimeter-wave frequencies.

References

1. Jantunen H, Hu T, Uusimäki A & Leppävuori S (2004) Tape casting of ferroelectric, dielectric, piezoelectric and ferromagnetic materials. *J Eur Ceram Soc* 24(6): 1077–1081.
2. Bray JR, Kautio KT & Roy L (2004) Characterization of an experimental ferrite LTCC tape system for microwave and millimeter-wave applications. *IEEE Trans Adv Packag* 27(3): 558–565.
3. Matters-Kammerer M, Mackens U, Reimann K, Pietig R, Hennings D, Schreinemacher B, Mauczok R, Gruhlke S & Martiny C (2006) Material properties and RF applications of high k and ferrite LTCC ceramics. *Microelectron Reliab* 46(1): 134–143.
4. Feingold AH, Heinz M & Wahlers RL (2003) Dielectric & Magnetic Materials for Integrated Passives. *Proc IMAPS Ceramic Interconnect Technology – The Next Generation Conference, Denver, USA*: 189–194.
5. Higuchi Y, Sugimoto Y, Harada J & Tamura H (2007) LTCC system with new high- ϵ_p and high-Q material co-fired with conventional low- ϵ_r base material for wireless communications. *J Eur Ceram Soc* 27(8–9): 2785–2788.
6. Hu T, Jantunen H, Uusimäki A & Leppävuori S (2002) Ba_{0.7}Sr_{0.3}TiO₃ powders with B₂O₃ additive prepared by the sol–gel method for use as microwave material. *Mater Sci Semicond Process* 5(2–3): 215–221.
7. Rhim SM, Hong S, Bak H & Kim OK (2000) Effects of B₂O₃ Addition on the Dielectric and Ferroelectric Properties of Ba_{0.7}Sr_{0.3}TiO₃ Ceramics. *J Am Ceram Soc* 83: 1145–1148.
8. Valant M & Suvorov D (2004) Low-Temperature Sintering of (Ba_{0.6}Sr_{0.4})TiO₃. *J Am Ceram Soc* 87(7): 1222–1226.
9. Jantunen H, Hu T, Uusimäki A & Leppävuori S (2004) Ferroelectric LTCC for Multilayer Devices. *J Jpn Ceram Soc* 112: 1552–1556.
10. Deleniv A, Hu T, Jantunen H, Leppävuori S & Gevorgian S (2003) Tunable ferroelectric components in LTCC technology. *Proc IEEE MTT-S International Microwave Symposium Digest, Philadelphia, USA* 3: 1997–2000.
11. Rentsch S, Hu T, Müller J, Stephan R, Hein M & Jantunen H (2007) Tunable Dielectric Material Embedded in LTCC for GHz-Frequency-Range Applications. *Proc European Microelectronics and Packaging Conference & Exhibition, Oulu, Finland*: 290–294.
12. Su B & Button TW (2001) Interactions between barium strontium titanate (BST) thick films and alumina substrates. *J Eur Ceram Soc* 21(15): 2777–2781.
13. Stove AG (1992) Automotive radar at 80–90 GHz. *Proc IEEE MTT-S International Microwave Symposium Digest, Albuquerque, USA* 2: 613–616.
14. Lo DCW, Yujiri L, Dow GS, Ton TN, Mussetto M & Allen BR (1994) A W-band direct-detection radiometric imaging array. *Proc Microwave and Millimeter-Wave Monolithic Circuits Symposium Digest, San Diego, USA*: 41–44.

15. Lucyszyn S, Silva SRP, Robertson ID, Collier RJ, Jastrzebski AK, Thayne IG & Beaumont SP (1998) Terahertz multi-chip module (T-MCM) technology for the 21st century? IEE Colloquium on Multi-Chip Modules and RFICs (Ref. No. 1998/231): 6/1–6/8.
16. Stephens D, Young PR & Robertson ID (2005) Millimeter-wave substrate integrated waveguides and filters in photoimageable thick-film technology. *IEEE Trans Microwave Theory Tech* 53(12): 3832–3838.
17. Rong Y, Zaki A, Gipprich J, Hageman M & Stevens D (1999) LTCC wide-band ridge-waveguide bandpass filters. *IEEE Trans Microwave Theory Tech* 47(9): 1836–1840.
18. Deslandes D & Wu K (2003) Single-substrate integration technique of planar circuits and waveguide filters. *IEEE Trans Microwave Theory Tech* 51(2): 593–596.
19. Hao ZC, Hong W, Chen XP, Chen JX, Wu K & Cui TJ (2005) Multilayered substrate integrated waveguide (MSIW) elliptic filter. *IEEE Microwave Compon Lett* 15(2): 95–97.
20. Aftanasar MS, Young PR & Robertson ID (2002) Rectangular Waveguide Filters Using Photoimageable Thick-film Processing. *Proc 32nd. European Microwave Conference, Milan, Italy*: 1–4.
21. Stephens D, Young PR & Robertson ID (2005) Design and characterization of 180 GHz filters in photoimageable thick-film technology. *Proc IEEE MTT-S International Microwave Symposium Diges, Long Beach, USA*: 4.
22. Yan L, Hong W, Hua G, Chen JX, Wu K & Cui TJ (2004) Simulation and experiment on SIW slot array antennas. *IEEE Microwave Compon Lett* 14(9): 446–448.
23. Stephens D, Young PR & Robertson ID (2005) W-band substrate integrated waveguide slot antenna. *Electronics Letters* 41(4): 165–167.
24. Wenquan C, Yung EK- & Wu K (2003) Millimeter-wave ferrite phase shifter in substrate integrated waveguide (SIW). *Proc IEEE Antennas and Propagation Society International Symposium, Columbus, USA* 4: 887–890.
25. D'Orazio W, Wu K & Helszajn J (2004) A substrate integrated waveguide degree-2 circulator. *IEEE Microwave Compon Lett* 14(5): 207–209.
26. Digby JW, McIntosh CE, Parkhurst GM, Towlson BM, Hadjiloucas S, Bowen JW, Chamberlain JM, Pollard RD, Miles RE, Steenson DP, Karatzas LS, Cronin NJ & Davies SR (2000) Fabrication and characterization of micromachined rectangular waveguide components for use at millimeter-wave and terahertz frequencies. *IEEE Trans Microwave Theory Tech* 48(8): 1293–1302.
27. Lucyszyn S, Wang QH & Robertson ID (1995) 0.1 THz rectangular waveguide on GaAs semi-insulating substrate. *Electronics Letters* 31(9): 721–722.
28. Aftanasar MS, Young PR, Robertson ID, Minalgiene J & Lucyszyn S (2001) Photoimageable thick-film millimetre-wave metal-pipe rectangular waveguides. *Electronics Letters* 37(18): 1122–1123.
29. Piloto AJ, Leahy KA, Flanick BA & Zaki KA (1995) Waveguide filters having a layered structure. *US Patent 5,382,931*

30. Uchimura H, Takenoshita T & Fujii M (1998) Development of a “laminated waveguide”. *IEEE Trans Microwave Theory Tech* 46(12): 2438–2443.
31. Diamond H (1961) Variation of Permittivity with Electric Field in Perovskite-Like Ferroelectrics. *J Appl Phys.* 32(5): 909–915.
32. Liou J & Chiou B (1997) DC Field Dependence of the Dielectric Characteristics of Doped Ba_{0.65}Sr_{0.35}TiO₃ with Various Grain Sizes in the Paraelectric State. *Jpn J Appl Phys* 36: 4359–4368.
33. Lemanov VV, Smirnova EP, Syrnikov PP & Tarakanov EA (1996) Phase transitions and glasslike behavior in Sr_{1-x}BaxTiO₃. *Phys Rev B* 54(5): 3151–3157.
34. Zhang L, Zhong L, Wang CL, Zhang PL & Wang YG (1998) Dielectric Properties of Ba_{0.7}Sr_{0.3}TiO₃ Ceramics with Different Grain Size. *Phys Stat Sol (a)* 168(2): 543–548.
35. Fang T, Hsieh H & Shiau F (1993) Effects of Pore Morphology and Grain Size on the Dielectric Properties and Tetragonal-Cubic Phase Transition of High-Purity Barium Titanate. *J Am Ceram Soc* 76(5): 1205–1211.
36. Johnson KM (1962) Variation of Dielectric Constant with Voltage in Ferroelectrics and Its Application to Parametric Devices. *J Appl Phys* 33(9): 2826–2831.
37. Palukuru VK, Komulainen M, Tick T, Perantie J & Jantunen H (2008) Low-Sintering-Temperature Ferroelectric Thick Films; RF Properties and an Application in a Frequency-Tunable Folded Slot Antenna. *IEEE Antennas Wirel Propag Lett* 7: 461–464
38. Palukuru VK, Perantie J, Komulainen M, Tick T & Jantunen H (2009) Tunable microwave devices using low sintering temperature screen printed Barium Strontium Titanate (BST) thick films. *J Eur Ceram Soc* DOI: 10.1016/j.jeurceramsoc.2009.07.003. (in press)
39. Palukuru VK, Perantie J, Komulainen M, Tick T, Jäntti J & Jantunen H (2009) In-band frequency-tunable ceramic planar inverted-F antenna (PIFA) utilizing an integrated BST-based variable capacitor. *Ferroelectrics* 388(1): 10-16.
40. Ouaddari M, Delprat S, Vidal F, Chaker M & Ke Wu (2005) Microwave characterization of ferroelectric thin-film materials. *IEEE Trans Microwave Theory Tech* 53(4): 1390–1397.
41. Mikeska KR, Schaefer DT & Jensen RH (1991) Method for reducing shrinkage during firing of green ceramic bodies. US Patent 005,085,720A
42. Clegg WJ, Kendall K, Alford NM, Button TW & Birchall JD (1990) A simple way to make tough ceramics. *Nature* 347(6292): 455–457.
43. Imhof H & Schless T (2004) Ceramic Interconnect Initiative (CII) Technology Roadmap.
44. Wang G, Folk EC, Barlow F & Elshabini A (2006) Fabrication of microvias for multilayer LTCC substrates. *IEEE Trans Electron Packag Manuf* 29(1): 32–41.
45. Haertling C, Shapiro AA, Goodman CA, Pond RG, Washburn RD, McClanahan RF, Gonzales CH & Lusher DM Low-Temperature-Cofired-Ceramic (LTCC) tape structures including cofired ferromagnetic elements, drop-in components and multi-layer transformer. US Patent 5,532,667

46. McClanahan RF & Washburn RD Dielectric vias within multi-layer 3-dimensional structures/substrates. US Patent 5,354,599
47. Smith HD, McClanahan RF, Shapiro AA & Brown R Via resistors within-multi-layer, 3 dimensional structures substrates. US Patent 5,164,699
48. Xu F & Wu K (2005) Guided-wave and leakage characteristics of substrate integrated waveguide. *IEEE Trans Microwave Theory Tech* 53(1): 66–73.
49. Li H, Hong W, Cui TJ, Wu K, Zhang YL & Yan L (2003) Propagation characteristics of substrate integrated waveguide based on LTCC. *Proc IEEE MTT-S International Microwave Symposium Digest, Philadelphia, USA* 3: 2045–2048.
50. Birol H, Maeder T & Ryser P (2007) Application of graphite-based sacrificial layers for fabrication of LTCC (low temperature co-fired ceramic) membranes and micro-channels. *J Micromech Microengineering* 17(1): 50–60.
51. Birol H, Maeder T, Jacq C, Straessler S & Ryser P (2005) Fabrication of low-temperature co-fired ceramics micro-fluidic devices using sacrificial carbon layers. *Int J Appl Ceram Technol* 2(5): 364–373.
52. Golonka LJ, Zawada T, Radojewski J, Roguszczyk H, Stefanow M (2006) LTCC Microfluidic System. *Int J Appl Ceram Technol* 3(2): 150–156.
53. Barlow F, Wood J, Elshabini A, Stephens EF, Feeler R, Kemner G & Junghans J (2009) Fabrication of precise fluidic structures in LTCC. *Int J Appl Ceram Technol* 6(1): 18–23.

Original papers

- I Tick T, Peräntie J, Jantunen H & Uusimäki A (2008) Screen printed low-sintering-temperature barium strontium titanate (BST) thick films. *Journal of the European ceramic society* 28: 837–842.
- II Tick T, Peräntie J, Rentsch S, Müller J, Hein M & Jantunen H (2008) Co-sintering of barium strontium titanate (BST) thick films inside a LTCC substrate with pressure-assisted sintering. *Journal of the European ceramic society* 28: 2765–2769.
- III Tick T, Palukuru V, Komulainen M, Peräntie J & Jantunen H (2008) Method for manufacturing embedded variable capacitors in low-temperature cofired ceramic substrate. *IEEE Electronics Letters* 44: 94–95.
- IV Tick T, Jäntti J, Henry M, Free C & Jantunen H (2009) LTCC integrated air-filled waveguides for G-band applications. *Microwave and optical technology letters* 51: 176–178.
- V Henry M, Osman N, Tick T & Free C (2008) Integrated Air-Filled Waveguide Antennas in LTCC for G-band operation. *Proc Asia Pacific Microwave Conference (APMC)*, Hong Kong, China.

Published papers have been reprinted with permission from Elsevier B.V. (I, II), IEEE/IET (III), John Wiley & Sons, Inc. (IV) and APMC (V).

Original publications are not included in the electronic version of the thesis.

ACTA UNIVERSITATIS OULUENSIS
SERIES C TECHNICA

322. Liedes, Toni (2009) Improving the performance of the semi-active tuned mass damper
323. Marina Tyunina & Orest Vendik (Eds.) (2009) Proceedings of the 16th International Student Seminar "Microwave and optical applications of novel phenomena and technologies", June 8–9, Oulu, Finland
324. Belt, Pekka (2009) Improving verification and validation activities in ICT companies—product development management approach
325. Harri Haapasalo & Hanna Kropsu-Vehkaperä (Eds.) (2009) The 3rd Nordic Innovation Research Conference - NIR 2008—IEM Arctic Workshop
326. Selek, István (2009) Novel evolutionary methods in engineering optimization—towards robustness and efficiency
327. Härkönen, Janne (2009) Improving product development process through verification and validation
328. Peiponen, Kai-Erik (2009) Optical spectra analysis of turbid liquids
329. Kettunen, Juha (2009) Essays on strategic management and quality assurance
330. Ahonen, Timo (2009) Face and texture image analysis with quantized filter response statistics
331. Uusipaavaliemi, Sari (2009) Framework for analysing and developing information integration. A study on steel industry maintenance service supply chain
332. Risikko, Tanja (2009) Safety, health and productivity of cold work. A management model, implementation and effects
333. Virtanen, Markku (2009) Mathematical modelling of flow and transport as link to impacts in multidiscipline environments
334. Liimatainen, Henrikki (2009) Interactions between fibres, fines and fillers in papermaking. Influence on dewatering and retention of pulp suspensions
335. Ghaboosi, Kaveh (2009) Intelligent medium access control for the future wireless networks
336. Möttönen, Matti (2009) Requirements engineering. Linking design and manufacturing in ICT companies
337. Leinonen, Jouko (2009) Analysis of OFDMA resource allocation with limited feedback

Book orders:
OULU UNIVERSITY PRESS
P.O. Box 8200, FI-90014
University of Oulu, Finland

Distributed by
OULU UNIVERSITY LIBRARY
P.O. Box 7500, FI-90014
University of Oulu, Finland

S E R I E S E D I T O R S

A
SCIENTIAE RERUM NATURALIUM

Professor Mikko Siponen

B
HUMANIORA

University Lecturer Elise Kärkkäinen

C
TECHNICA

Professor Hannu Heusala

D
MEDICA

Professor Helvi Kyngäs

E
SCIENTIAE RERUM SOCIALIUM

Senior Researcher Eila Estola

F
SCRIPTA ACADEMICA

Information officer Tiina Pistokoski

G
OECONOMICA

University Lecturer Seppo Eriksson

EDITOR IN CHIEF

University Lecturer Seppo Eriksson

PUBLICATIONS EDITOR

Publications Editor Kirsti Nurkkala

ISBN 978-951-42-9249-1 (Paperback)

ISBN 978-951-42-9250-7 (PDF)

ISSN 0355-3213 (Print)

ISSN 1796-2226 (Online)

